Impact Of Iron Dopant on The Structural and Electrical Characteristics of Zirconium Oxide (ZrO_2)

N.N. Gour[1], H.G. Wankhade[2], P. R. Padole[3]
[1,2,3]*Department of Chemistry, Shri Shivaji Science College Amravati. (MS) India 444601*

***Abstract*—The sol-gel citrate method was used to synthesize nanocrystalline zirconium oxide (ZrO_2). It was further modified by Fe metal doping. both modified and unmodified ZrO_2 were subjected to structural and electrical analysis. In X-ray diffraction (XRD) studies, the average crystallite size of undoped ZrO_2 was found to be 46 nm. When ZrO_2 is doped with 0.1%, 0.2% and 0.3% Fe its average crystallite size decreases to 45, 30, and 20 nm respectively. Particle size and morphology were examined using a scanning electron microscope (SEM). Dielectric properties of ZrO_2 nanoparticles were performed at different temperatures. The change of dielectric constant and di- electric loss were studied. The dielectric constants of ZrO_2 nanoparticles are high at low frequencies and decrease rapidly as the frequency increases. Electrical analysis of nanocrystalline zirconia is performed for each sample at different temperature and with a different Fe doping level. Research shows that conductivity varies depending on temperature and the content of impurities. SEM studies showed the development of agglomerated crystals.**

***Index Terms*—Zirconium oxide nanoparticles, X-ray diffraction, Crystallite size, SEM analysis, Dielectric constant and Dielectric loss, Electrical Properties and Conductivity.**

I. INTRODUCTION

Some of the commonly used synthetic methods are non-sputtering, solve thermal, reduction, hydrothermal technique, and electrochemical techniques. However, these techniques are expensive, poisonous, and take a lot of energy and pressure. They are also challenging to separate and may be dangerous [1]. However, the Sol-gel process is an inexpensive, non-toxic way to generate nanoparticles that can be used theoretically safely, and with great ease. Zirconium dioxide with its unique physical and chemical features like hardness, ionic conductivity, and surface activity is a promising material that is widely employed as supports solid electrolytes and catalysts [2-4]. The technical performance and physico-chemical characteristics of ZrO_2 are significantly influenced by crystalline structures, including flaws, crystal phases, and crystallite sizes [5-7]. Because of its excellent thermal stability (1WmK) oxygen ion conductivity, small size, vast surface area, low cost, amphoteric features, and redox capabilities, ZrO_2 has garnered a lot of attention recently [8-11]. Zirconia is a more stable semiconducting metal oxide than other oxides.

Zirconium oxide is a wide band gap metal oxide having interesting applications such as structural ceramic [12], catalytic support [13], oxygen sensor [14], fuel cell [15], thermal barrier coatings [16], dielectric in metal oxide semiconductor (MOS) devices [17-18], optoelectronics and data storage, photonics and dilute magnetic Oxides (DMOs) in spintronics [19-20]. One useful method for considerably altering metal oxide is doping. Cations such as Fe^{2+}, Cu^{2+}, Zn^{2+}, and so forth are capable of effectively reducing ZrO_2's large band gap. Fe is one of the best options for doping ZrO_2 since it not only improves light harvesting efficiency but also adds room temperature ferromagnetism to the host lattice. The semiconductor zirconium oxide (ZrO_2) has a broad straight band gap and regarded as a multipurpose material because of its exceptional mechanical, chemical and thermal durability as well as its non-toxicity and adsorption capacity. It was applied in numerous scientific and technological domains, including dentistry, biology, electronics, optics, magnetism, adsorption, catalysis, and optics.[21]

II. LITERATURE SURVEY RELATED TO DOPANT

Enza Fazio et al. in his review discussed and summarized the pure, mixed and doped metal oxide semiconductor-based electrical and electrochemical sensors used for gas sensing and for the determination

of electroactive biomolecules are described in terms of their sensing performance and their practical limitations to be used for multi-detections of gases and analytes [29].

Sachin Kumar et al investigated the effect of calcination temperature from 500 to 700 °C on the Zirconia (ZrO_2)

One useful method for considerably altering metal oxide is doping. Cations such as Fe^{2+}, Cu^{2+}, Zn^{2+}, and so forth are capable of effectively reducing ZrO_2's large band gap. Fe is one of the best options for doping ZrO_2 since it not only improves light harvesting efficiency but also adds room-temperature ferromagnetism to the host lattice. The semiconductor zirconium oxide (ZrO_2) has a broad straight band gap and is regarded as a multipurpose material because of its exceptional mechanical, chemical, and thermal durability as well as its non-toxicity and adsorption capacity.

It was applied in numerous scientific and technological domains including dentistry, biology, electronics, optics, magnetism, adsorption, catalysis, and optics [30].

Yacine Cherifi et al. reviewed and compiled Fe-doped ZnO_2 nanoparticles using the sol-gel citrate technique in their review. Additional nanoparticle structure is revealed by various characterisation methods. Complex impedance spectroscopy was used to examine the electric and dielectric characteristics. Fe appears to be positively involved in the separation of photo-generated electron-hole pairs, as evidenced by the greater activity of the Fe-doped ZnO_2 products compared to the pure ZnO_2 [31].

Waheed Ahmed et al. summarized the, synthesis, characteristics, dielectric properties and photocatalytic activity of undoped and Fe doped ZrO_2 nanoparticles. The Fe dopant enhanced the dielectric constant of ZrO_2 nanoparticles as compare to pure ZrO_2. So this nanoparticles are applicable to spintronics, high-frequency devices, and water purifications technologies [32].

In this manuscript, Impact of Iron Dopant on the Structural and Electrical Characteristics of Zirconium Oxide (ZrO_2)

III. EXPERIMENTAL METHOD

The materials such as Zirconium Nitrate, Ferric Nitrate, Citric acid and Ethylene Glycol were used in the synthesis of undoped & Fe doped Zirconium oxide (ZrO_2) nano particles using sol-gel method. The precursor materials are of AR grade and used as it is.

Synthesis of Copper Oxide Nano particles

The sol-gel method was utilized to create unalloyed and Fe-doped zirconium oxide (ZrO_2) nano particles using materials including ferric nitrate, citric acid, and ethylene glycol. The source materials employed in the synthesis of zirconium oxide nano particles are of grade AR. Using the sol-gel citrate technique, a stoichiometric quantity of Zr $(NO_3)_2$. H_2O was dissolved in ethylene glycol to create nano crystalline zirconium oxide. After being agitated for three hours at 80°C to create a homogenous mixture, the mixture was heated for an additional eight to twelve hours at 130°C in a pressure vessel to form gel formation. After that, the gel was calcined in a muffle furnace for three hours at 350°C in the oven.

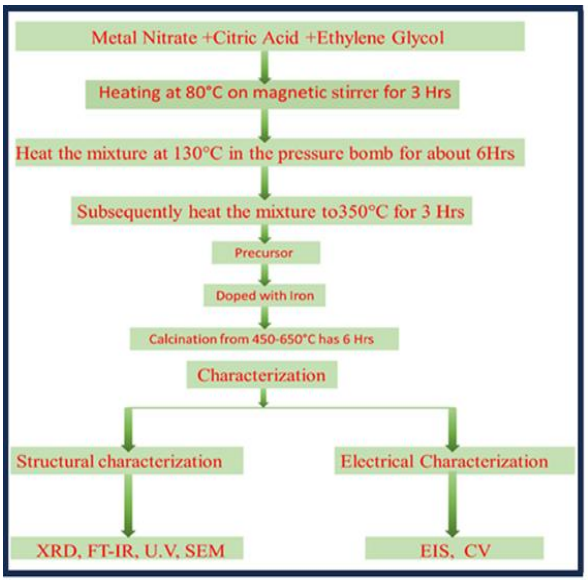

Fig.1: Sol-gel processes and Methodology

Characterizations Techniques

- An X-ray diffractometer with wavelength (1.5418A˚) (Rigaku, Japan) is used to analyse the structure of the sample. The sample is scanned for a 2θ (20-90°) range with a phase size of 0.020.
- For chemical analysis, an IR spectrometer in the range of wave numbers 400-4000 cm^{-1} and a

resolution of 0.5 cm^{-1} (SHIMADU) is used to confirm the chemical bonds of the sample.

- A scanning electron microscope (Carl Zeiss microscopy Ltd, UK & SIGMA) was used to analyse the morphology and composition.
- Electrochemical analysis was performed using CHI608E workstation (Electrical Potential) Series was used to analyse Conductance.
- Electrochemical analysis was performed using (Conductance) (HIOKI characterization impedance 3532-50) LCR HITESTER Made in Japan) was used to analyse Conductance.

IV. RESULT & DISCUSSION

4.1. X-ray Diffraction

X-ray diffraction study is carried out to determine the structure, crystallinity, and crystallite size of the ZrO_2 Nanoparticles in the 2θ° range of 20-90°. The XRD pattern of undoped (FS1) and 0.1%, 0.2% and 0.3% Fe doped ZrO_2 nano particles (FS2-FS4) at a temperature of 550°C is shown in Fig. 3.2 (FS1-FS4). From XRD studies it was observed that the average particle size of Sample FS1 is 46 nm, according to X-ray diffraction (XRD) research. The average crystallite size of Sample FS2, FS3 and FS4 is 45 nm, 30 nm and 20 nm, respectively.

The Scherrer formula was used to measure the crystallite sizes from the peak of the XRD pattern from the FWHM [22, 23],

$D = k \lambda / \beta \cos \theta$……(1)

Where D is the average size of the crystallite, assuming that the grain is spherical, k is 0.9, λ is the wavelength of X-ray radiation, β is the (FWHM), θ is the angle of diffraction pattern. In general, doping decreases the size of nano particles and the also intensity of the X-ray diffraction (XRD) peak. This is due to a change in electron density, point defects, lattice distortion, and grain refinement. Doping changes, the element, which changes the mean atomic scattering factor on a given site [24]. doped ZrO_2 was monoclinic phase determined in XRD Data.

The presence of sharp and intense XRD peaks in both the pure and Fe-doped Zirconium Oxide samples indicates their high-quality crystal structure and excellent crystallinity. The sharp peaks appearing at 30.24°, 33.52°, 50.29°, 60.74°, 74.11° and 77.79 °correspond to the (111), (200), (220), (311), (400), and (420) planes, respectively, confirming the occurrence of monoclinic and Tetragonal phases [25-26].

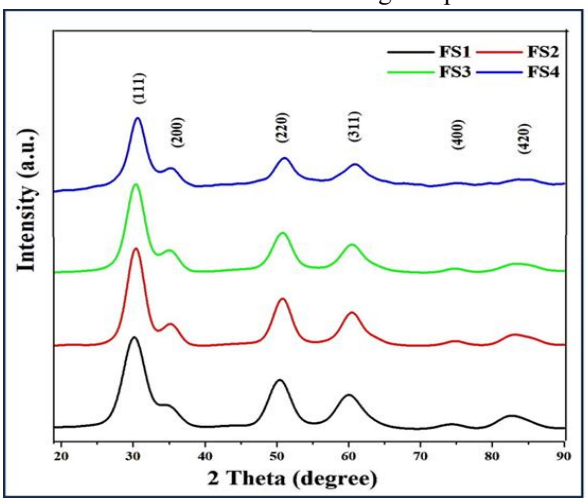

Fig. 2: XRD plot for (a) undoped ZrO_2, (b) 0.1% Fe, (c) 0.2 % Fe, (d) 0.3 % Fe doped ZrO_2.

The diffractometric analysis of Fe-doped ZrO_2 showed that tausonite (ICCD No. 98–005–6717) was the only phase present in the pristine and Fe-doped ZrO_2 samples. Furthermore, these sharp peaks and the absence of any impurity peaks in samples FS2-FS4 indicate a relatively high solubility limit for Fe in the Zirconium structure [24].

4.2. FT-IR Studies

A Fourier-transformed infrared (FTIR) investigation was performed to examine ZrO_2 surface chemistry in detail. Fig. 3.3 displays the FTIR spectra of the undoped and Fe-doped ZrO_2 nano composite samples denoted as FS1, FS2, FS3, and FS4 (ZrO2, 01, 0.2, 0.3 FeZrO2). The prominent peaks obtained at 3427.21 cm^{-1} and 1627.09 cm^{-1} in the FTIR spectrum are indicative of the O-H bond's stretching and bending vibrations [24]. These bands are characteristic of water molecules (H_2O) or hydroxyl groups (-OH) adsorbed on the surface or incorporated into the lattice structure of the material. The peak at 1394.01-1521.23 cm-1 is due to the vibration of C-H bending [27]. The distinctive bands of ZrO2 often show up between 400 and 600 cm^{-1}, due to the stretching vibration of Zr-O bonds, which indicates that the ZrO2 units have Tetragonal symmetry, while peaks observed at 853.6-1068.32 cm-1 belongs to the stretching mode of Zr = O. Hence, it is confirmed that FTIR spectroscopy can effectively be used to examine the crystalline phase of zirconia nano particles [28].

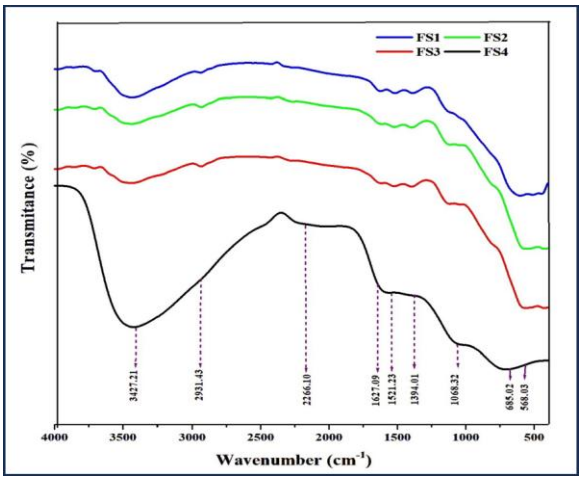

Fig. 3. FT-IR plot for (FS1-FS4) undoped & 0.1, 0.2, 0.3% Fe doped ZrO_2

Zr-O bond vibrations may be represented as peaks in the 600–700 cm^{-1} range, indicating the involvement of Zirconium in the structure. There are slight shifts in the peak positions across the samples (FS2 to FS4) towards lower wavelength regions, suggesting structural or compositional modifications due to Fe-doping. Fe-doping likely introduces lattice distortions or affects the local chemical environment, altering the vibrational modes. Thus, ZrO_2 and Iron-doped ZrO_2 nano composites were effectively produced, according to the analytical findings [24].

4.3. Scanning Electron Microscope (SEM)

FESEM images show the surface morphology of the zirconiumum oxide nanoparticles (Fig.3.4). It shows the well-defined formation of the crystallites with different magnifications. The crystallitesare agglomerated and formed a cluster Fig. 3.4 (a). ZrO_2 nano particles were aggregated in the form of nano disc/plate shapes [24]. A significant shift in the morphological parameter was noted when the Fe doping ratio was changed from 0.1 to 0.3 % (i.e., 0.1%,0.2%, and 0.3%). The prepared sample exhibits spherical shaped particles, while sample exhibits uniformly homogenous more regular spherical shape as compare to ZrO_2, as demonstrated by the micrographs Fig. 4 (b-d). Lighter particles (bright portion) were detected dispersed over the surface of the zirconia which was assigned to iron oxide nano particles. Lighter elements tend to absorb electrons, making them look bright, while heavy elements actively backscatter electrons, making those areas appear darken [24]. According to the histogram probability diagrams in Fig.4 (e-h), the average particle sizes of pure zirconia is 48.26 nm and 0.1, 0.2, 0.3% Fe doped zirconia were 41.24 nm, 32.85 nm, 28.37 nm respectively.

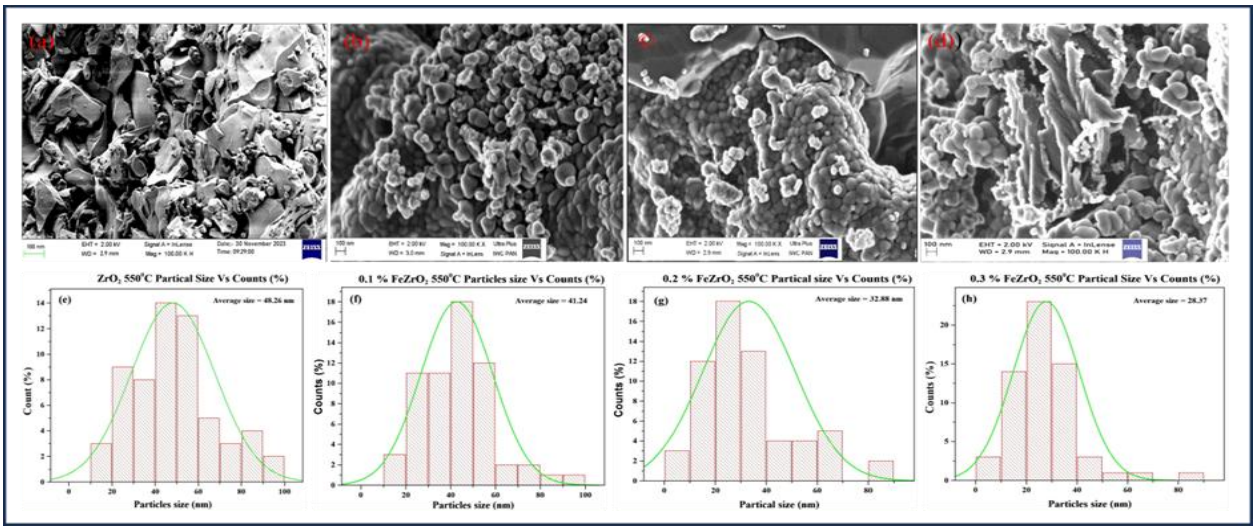

Fig.4. SEM images (a-d) Pure & Fe doped ZrO2, (e-h) Average particle size pure and Fe doped ZrO2.

Electrochemical analysis

a). Cyclic voltammetry (CV) study

Cyclic voltammetry (CV) was performed to investigate the electrochemical properties of Iron-doped ZrO_2 (Fe-ZrO_2) nanoparticles. The measurements were carried out using a standard three-electrode system, consisting of a glassy carbon electrode (GCE) as the working electrode, a platinum wire as the counter electrode, and Ag/AgCl as the reference electrode. The electrolyte used was 1 M

Na_2SO_4 aqueous solution. Prior to measurement, the working electrode was modified by drop-casting a dispersion of the synthesized Fe-ZrO_2 nanoparticles in ethanol and Nafion binder, followed by drying at room temperature.

The CV curves were recorded within a potential window of -0.2 V to + 0.8 V (vs. Ag/AgCl) at various scan rates ranging from 5 to 100 mV/s. The electrochemical behavior of Fe-ZrO_2 was compared with that of pure ZrO_2 to examine that effect of Fe doping on the redox activity and charge storage capability [29]. Electrochemical investigations of the as prepared electrodes were carried out using CV and EIS.

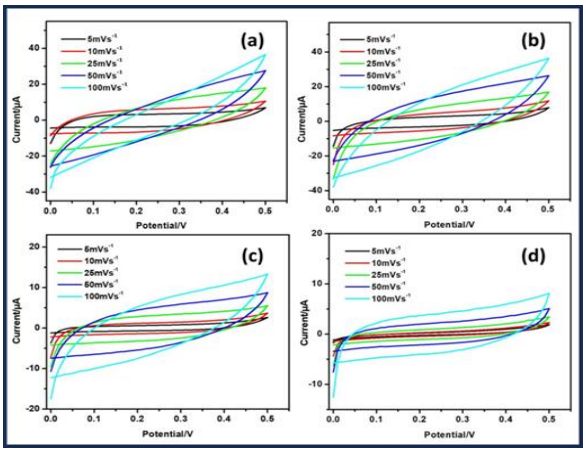

Fig. 5. Cyclic voltammogram of (a) FS1, (b) FS2, (c) FS3, and (d) FS4 at different scan rates

The CV curves of samples FS1, FS2, FS3, and FS4 (a-d) showed that while the size and shape are almost comparable. From the CV study is observe that the samples FS1, FS2, FS3, and FS4. Out of the different samples, sample FS3 demonstrated excellent electrochemical performance and resulted in a high specific capacitance reaching 510 F/g at a scan rate of 5 mV/s. Fig. 5 represents the variation in Cs vs. the scan rate, which shows that the specific capacitance of the electrodes decreased at a higher scan rate. The peak potential having a positive shift, it can be noted that peak current enhancement is based on increased electroactive surface area brought about by the 0.2% $FeZrO_2$ nanoparticles. The amorphous ZrO_2 nanoparticles used for the modification of CPE increased the electroactive surface area of the electrode about eight-fold; from 0.0345 cm^2 to 0.276 cm^2. The positive shift of the peak potential produced by the zirconia nanoparticles by modified electrode shows in sample (FS2-FS4) an increase over potential, possibly as a result of the modification. If the modified electrode acted as an electro-catalyst, there would have been a reduction of peak potential. The reduction of peak potential normally suggests a faster reaction with less over potential. Meanwhile, the lower the over potential, the better is the catalyst [30].

b). Impedance Analysis

The electronic transfer properties of nanocrystalline zirconium oxide after different surface modifications were characterized by using complex impedance spectroscopy (CIS) to understand the changes in electrical properties of the material over a wide range of frequencies. The conductivity of the sample was measured by an AC complex impedance method, and the applied frequency range of AC is from 42 Hz to 5 MHz [26, 31]. It can be noted from the study that conductivity varies with temperature and dopant concentration. The graph indicates that conductivity varies with temperature, with consistent changes only seen in ZrO_2 doped 0.2% Fe samples, which also have the highest conductivity of all the samples. The dielectric characteristics and AC conductivity of pure and Fe-doped ZrO_2 nanoparticles were studied at temperatures between 100°C and 700°C about a frequency range of 42 Hz to 500 KHz.

The conductivity (σ) for each constructed pallet is displayed as a frequency function (log F) in Fig.6. At low frequencies, conductivity values are extremely low and progressively increase as frequencies climb. It was also shown that the results improved at higher frequencies with an increase in laser ablation duration. Space charge polarization could be the primary reason for this evolution [31].

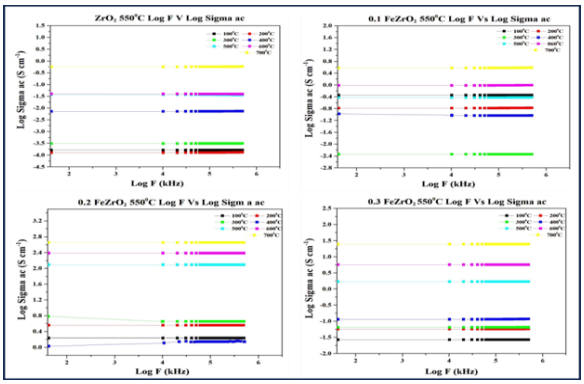

Fig. 6. The plot of Log (sigma ac) versus Log (F) different temperature for all prepared pure & 0.1, 0.2, 0.3 % Fe doped ZrO_2 pallet.

Fig. 7 Demonstrates the frequency dependence of the produced pallet on the dielectric constant ε' and dielectric loss Ɛ" depending on the addition of pure and Fe doped Zirconium oxide nanoparticles, the behaviour of ε" with frequency has two different regions. As seen in Fig.6 studied using a HIOKI 3532 LCR meter as a function of frequency (42 Hz – 100 kHz) at 100-700°C temperature. The complex dielectric of the materials has been provided as the formula by [31],

$$\varepsilon = \varepsilon' + j\varepsilon'' \quad \ldots\ldots\ldots\ldots\ldots\ldots\ldots\ldots(2)$$

Due to their low values at high frequencies, ε' and ε" were increased by prolonging the laser ablation period in the polymeric matrix, resulting in a constant value at high frequencies. This phenomenon is the result of polarization's effects [32]. The behavior of ε" with frequency exhibits two distinct areas, depending on the inclusion of Fe-doped and zirconium oxide nano particles.

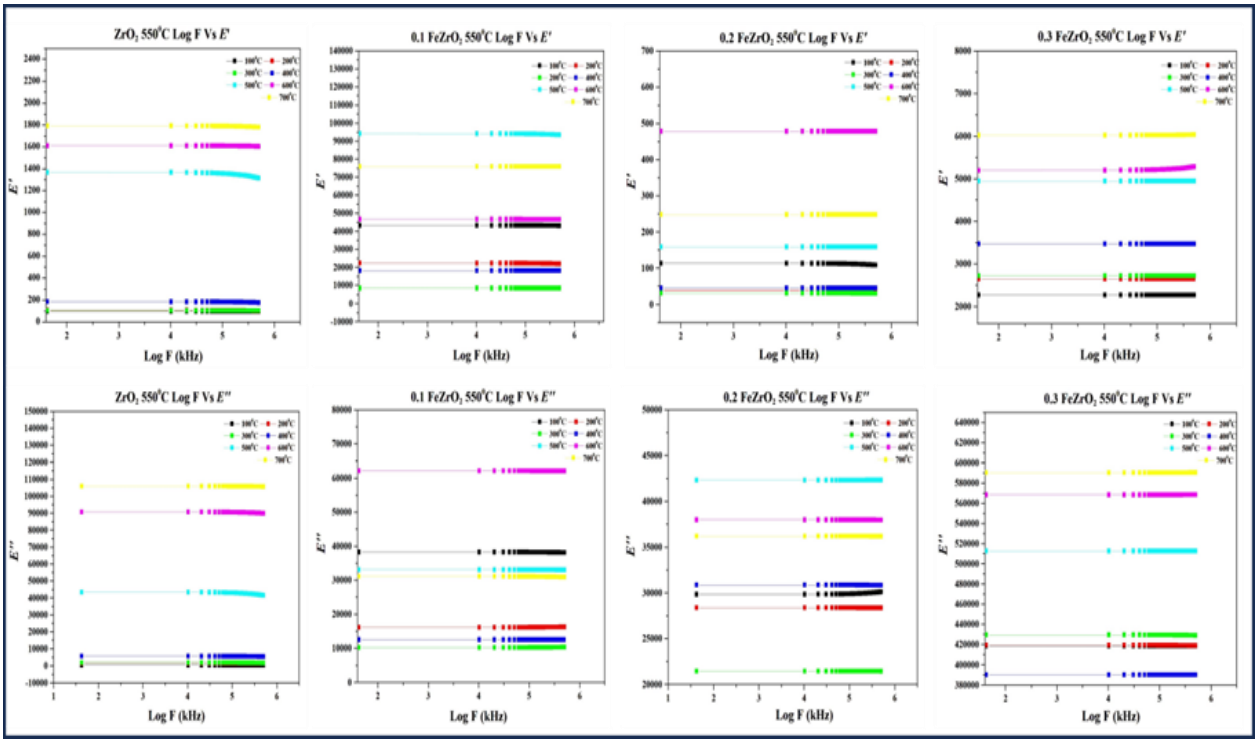

Fig. 7. Comparison of frequency-dependent real part ε′ and imaginary part ε″ of the complex dielectric permittivity for undoped and Fe doped ZrO_2 at 100° C to 700° C temperature.

The presence of two separate arcs in the complex impedance spectrum of (Z") versus (Z') indicates that the electrode polarization (EP) effect and bulk material properties may be distinguished using impedance spectroscopy [33]. Electrode polarization results from free charges building up at the interface between the dielectric materials and the electrode surface, which leads to the creation of electric double layer (E.D.L.) capacitance. The complex impedance of the nano composite samples can be determined using the relationship below;

$$Z^*(\omega) = Z' - JZ'' \quad \ldots\ldots\ldots\ldots\ldots\ldots(3)$$

If j is constant, Z' stands for the real component of the impedance, and Z" represents the imaginary component of the impedance. The variation of Z' with frequency for pure and Fe-doped zirconium oxide at temperatures between 100°C and 700°C is shown in Fig. 7 (a). Z' readings consistently decrease with increasing temperature and frequency, suggesting that the sac is growing [34]. In the high-frequency range, Z' values are nearly zero and independent of temperature. Fig. 8. illustrates the frequency-dependent changes in Z" for pure and Fe-doped zirconium oxide at different temperatures. The value of Z" declines with increasing frequencies at different temperatures, as Fig. 8. illustrates. The elevated Z" value of the nanocomposite samples may be due to a decrease in the space charge polarization process [35].

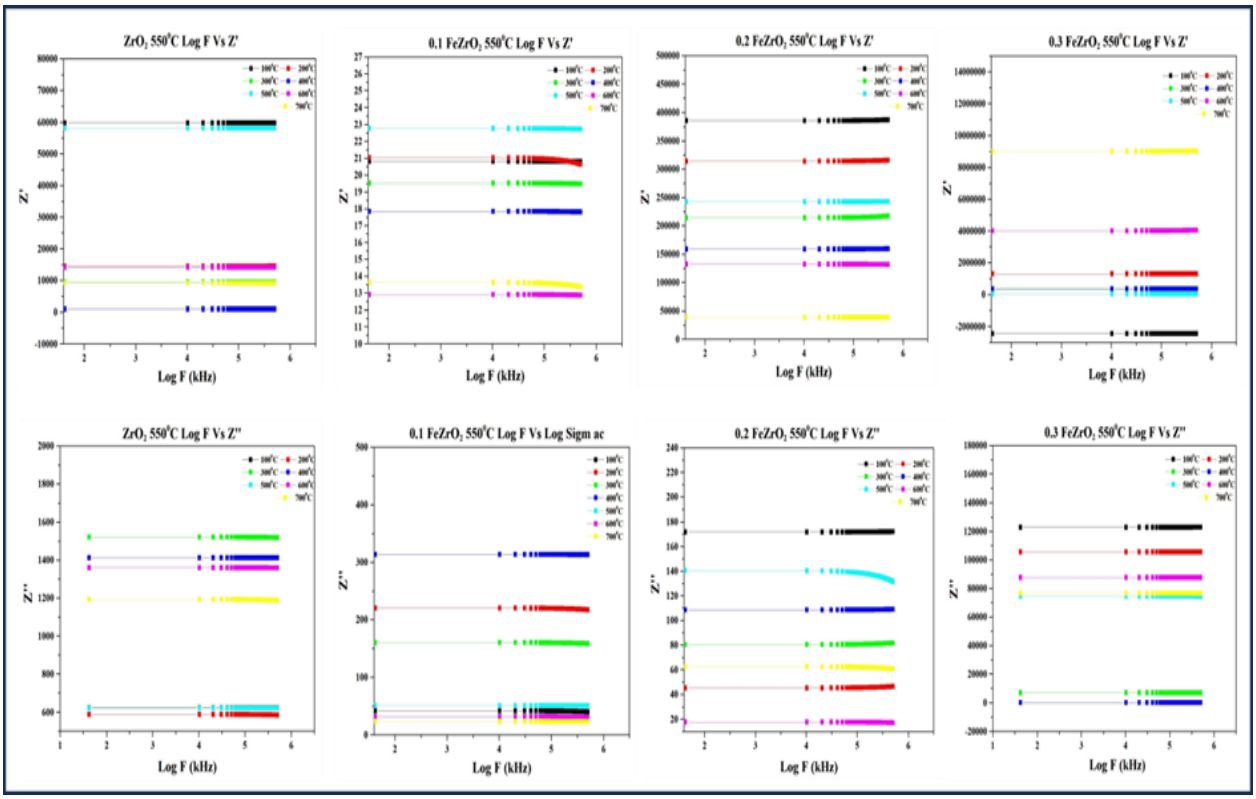

Fig. 8. The change of the Z′ of complex impedance as a function of Log (F) for pure and Fe doped ZrO_2, the change of the Z of complex impedance as a function of Log (F) for pure and Fe doped ZrO_2.

Impedance study for pure and Fe-doped ZrO_2 at 100°C to 700°C yields Nyquist plots of impedance spectra with a semicircle part, as illustrated in Fig. 9. The electron transfer restricted process is represented by the semicircle part at higher frequencies.

The semicircle's diameter can be used to calculate the electron transfer resistance at the electrode surface. The single semicircle seen in zirconia suggests that there are several possible routes for charge carrier migration, such as conduction across grains and grain boundaries or electrolyte-electrode contact.

The prepared Fe doped ZrO_2 shows two semicircles at 100°C and 500°C; at 400°C and above, the curve singles out. The resistance value fell as the temperature increased as shown by the impedance plot fitting. Zirconia only offers grain resistance at 100°C, while at temperatures beyond 500°C, it gives both grain and grain boundary resistance, according to capacitance values [36].

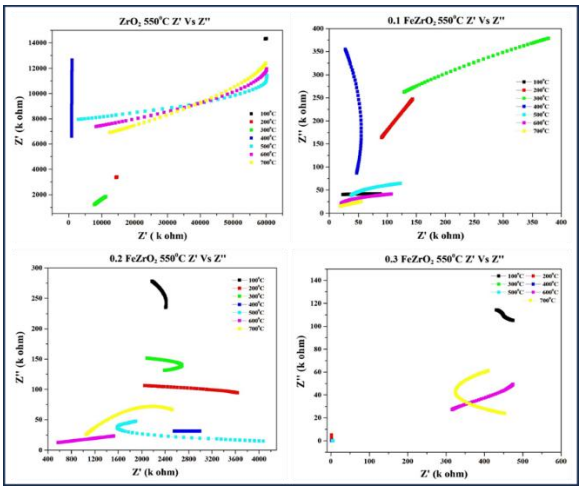

Fig. 9: The Nyquist plots of imaginary impedance (Z”) to the real impedance (Z’) of the prepared undoped and Fe doped ZrO_2 at various temperature.

V. CONCLUSION

In this study, the influence of iron (Fe) doping on the structural and electrical properties of zirconium oxide (ZrO_2) was systematically investigated. XRD and

SEM analyses tell that Fe dopant show that remarkable changes in the crystal structure, further phase stabilization and reducing crystallite size, which indicates the successful substitution of Fe into the ZrO_2 lattice. The observed lattice distortion suggests the formation of oxygen vacancies, which play a crucial role in modifying the material's electrical behaviour.

Electrical characterization demonstrated that Fe-doped ZrO_2 exhibits enhanced conductivity and reduced activation energy compared to undoped samples. This improvement can be attributed to increased charge carrier mobility resulting from defect engineering introduced by Fe doping. These findings suggest that Fe-doped ZrO_2 contain potential for applications in solid oxide fuel cells, gas sensors, and other electrochemical devices.

While the results confirm the beneficial effects of Fe doping, further studies are recommended to explore the long-term stability, optimal doping concentrations, and performance under usable conditions.

Further exploration and optimization of these materials could lead to advancements in areas such as environmental monitoring, medical diagnostics, and industrial process control

REFERENCES

[1] R. Prasad, K. M. Sharma, and A. Agrawal, "Synthesis and mass spectral studies of mixed ligand complexes of cobalt with 2-hydroxybenzophenone and β-diketones, hydroxyaryl aldehydes or ketones," *J. Indian Chem. Soc.*, vol. 84, no. 8, pp. 742–745, 2007.

[2] C. Chang and S. Yen, "Characterization of electrolytic ZrO_2/Al_2O_3 double-layer coatings on AISI 440C stainless steel," Surf. Coat. Technol., vol. 182, nos. 2–3, pp. 242–250, 2004.

[3] T. Politova and J. T. S. Irvine, "Investigation of scandia–yttria–zirconia system as an electrolyte material for intermediate-temperature fuel cells: Influence of yttria content in the $(Y_2O_3)x(Sc_2O_3)_{11-x}(ZrO_2)_{89}$ system," Solid State Ionics, vol. 168, nos. 1–2, pp. 153–165, 2004.

[4] M. De and D. Kunzru, "Oxidative dehydrogenation of propane on V_2O_5/ZrO_2 catalysts," Catal. Lett., vol. 96, pp. 33–42, 2004.

[5] T. Yamaguchi, "Application of ZrO_2 as a catalyst and a catalyst support," Catal. Today, vol. 20, no. 2, pp. 199–217, 1994.

[6] J. M. Grau, J. C. Yori, C. R. Vera, F. C. Lovey, A. M. Condó, and J. M. Parera, "Crystal phase-dependent metal–support interactions in $Pt/SO_4^{2-}–ZrO_2$ catalysts for hydroconversion of n-alkanes," Appl. Catal. A Gen., vol. 265, no. 2, pp. 141–152, 2004.

[7] G. Xu, Y.-W. Zhang, C.-S. Liao, and C.-H. Yan, "Grain size-dependent electrical conductivity in scandia-stabilized zirconia prepared by a mild urea-based hydrothermal method," Solid State Ionics, vol. 166, nos. 3–4, pp. 391–396, 2004.

[8] P. Arunkumar, U. Aarthi, M. Sri Balaji, B. Mukherjee, A. K. Keshri, W. H. Tanveer, S.-W. Cha, and K. S. Babu, "Deposition rate-dependent phase and mechanical property evolution in zirconia and ceria–zirconia thin films by EB-PVD technique," J. Alloys Compd., vol. 765, pp. 418–427, 2018.

[9] C. Amaya, J. Caicedo, J. Yañez Limón, R. Vargas, G. Zambrano, M. Gómez, and P. Prieto, "A non-destructive method for determination of thermal conductivity of YSZ coatings deposited on Si substrates," Mater. Chem. Phys., vol. 136, nos. 2–3, pp. 917–924, 2012.

[10] Y.-T. Foo, A. Z. Abdullah, B. A. Horri, and B. Salamatinia, "Ammonium oxalate-assisted synthesis of Gd_2O_3 nanopowders," Ceram. Int., vol. 45, no. 7, pp. 9082–9091, 2019.

[11] M. R. Loghman-Estarki, M. Hajizadeh-Oghaz, H. Edris, and R. S. Razavi, "Comparative studies on synthesis of nanocrystalline $Sc_2O_3–Y_2O_3$-doped zirconia (SYDZ) and YSZ solid solutions via modified and classic Pechini method," CrystEngComm, vol. 15, no. 29, pp. 5898–5909, 2013.

[12] S. Devgan and S. S. Sidhu, "Evolution of surface modification trends in bone-related biomaterials: A review," Mater. Chem. Phys., vol. 233, pp. 68–78, 2019.

[13] P. Baeza, G. Aguila, G. Vargas, J. Ojeda, and P. Araya, "Adsorption of thiophene and dibenzothiophene on highly dispersed Cu/ZrO_2 adsorbents," Appl. Catal. B Environ., vol. 111, pp. 133–140, 2012.

[14] E. P. Simonenko, A. S. Mokrushin, N. P. Simonenko, V. A. Voronov, V. P. Kim, S. V. Tkachev, S. P. Gubin, V. G. Sevastyanov, and N. T. Kuznetsov, "Ink-jet printing of a TiO_2–10% ZrO_2 thin film for oxygen detection using a

solution of metal alkoxy-acetylacetonates," Thin Solid Films, vol. 670, pp. 46–53, 2019.

[15] T. Selvaraj, B. Johar, and S. F. Khor, "Iron/zinc-doped 8 mol% yttria-stabilized zirconia electrolytes for green fuel cell technology: A comparative study of thermal analysis, crystalline structure, microstructure, mechanical and electrochemical properties," Mater. Chem. Phys., vol. 222, pp. 309–320, 2019.

[16] F. Saberi, B. S. Boroujeny, A. Doostmohamdi, A. R. Baboukani, and M. Asadikiya, "Electrophoretic deposition kinetics and properties of ZrO_2 nanocoatings," Mater. Chem. Phys., vol. 213, pp. 444–454, 2018.

[17] Y.-H. Wu, L.-L. Chen, W.-C. Chen, C.-C. Lin, M.-L. Wu, and J.-R. Wu, "MOS devices with tetragonal ZrO_2 as gate dielectric formed by annealing ZrO_2/Ge/ZrO_2 laminates," Microelectron. Eng., vol. 88, no. 7, pp. 1361–1364, 2011.

[18] J. U. Bhanu, A. Amutha, G. R. Babu, B. Sundaravel, and P. Thangadurai, "Crystalline phase-dependent electrical properties of Mg-incorporated tetragonal phase-stabilized ZrO_2 high-κ dielectric layers in Si-based MOS capacitors," Mater. Sci. Semicond. Process., vol. 81, pp. 7–16, 2018.

[19] G. R. Kumar, M. G. Krishna, and M. Rao, "Cr^{3+}-doped NaF–ZrO_2–B_2O_3–SiO_2 glass-ceramic materials for optoelectronic device applications," Optik, vol. 173, pp. 78–87, 2018.

[20] I. Ahmad, K. Alamgir, and I. H. Gul, "Structural, magnetic and dielectric characteristics of optically tuned Fe-doped ZrO_2 nanoparticles with visible-light-driven photocatalytic activity," Mater. Chem. Phys., vol. 251, Art. no. 122999, 2020.

[21] J. Zippel, M. Lorenz, A. Setzer, M. Rothermel, D. Spemann, P. Esquinazi, M. Grundmann, G. Wagner, R. Denecke, and A. Timopheev, "Defect-induced magnetism in homoepitaxial manganese-stabilized zirconia thin films," J. Phys. D: Appl. Phys., vol. 46, no. 27, Art. no. 275002, 2013.

[22] M. A. Aseel, F. H. Itab, and F. M. Ahmed, "Producing high purity metal oxide nanostructures using a simple chemical method," J. Phys.: Conf. Ser., vol. 1032, Art. no. 012036, 2018.

[23] A. M. Ferretti, S. Mondini, and A. Ponti, "Advances in colloid science for synthesis of nanoparticles," in Colloid Science, IntechOpen, 2016. doi: 10.5772/65092.

[24] T. Arul Vasanthi and G. Balakrishnan, "Synthesis of zirconium oxide nanoparticles and characterization," 2020, pp. 4955–4959, doi: 10.26637/MJM0S20/1278.

[25] S. Kumar, S. Bhunia, and A. K. Ojha, "Synthesis and characterization of zirconia-based nanomaterials," Physica E, vol. 66, pp. 74–80, 2015.

[26] Ch. V. Reddy, B. Babu, I. N. Reddy, and J. Shim, "Zirconia-based ceramic materials for advanced applications," Ceram. Int., vol. 44, pp. 6940–6948, 2018.

[27] A. A. Menazea, A. M. Abdelghany, N. A. Hakeem, W. H. Osman, and A. El-Kader, "Synthesis and characterization of zirconia nanomaterials," J. Ovonic Res., vol. 12, no. 4, pp. 277–286, 2016.

[28] M. R. Loghman-Estarki, H. Edris, and R. S. Razavi, "Large-scale synthesis of non-transformable tetragonal Sc_2O_3–Y_2O_3-doped ZrO_2 nanopowders via the citric acid-based gel method to obtain plasma-sprayed coatings," Ceram. Int., vol. 39, pp. 7817–7819, 2013.

[29] C. O. Chikere, N. H. Faisal, P. Kong-Thoo-Lin, and C. Fernandez, "The synergistic effect between graphene oxide nanocolloids and silicon dioxide nanoparticles for gallic acid sensing," J. Solid State Electrochem., vol. 23, pp. 1795–1809, 2019.

[30] C. O. Chikere, N. H. Faisal, P. Kong-Thoo-Lin, and C. Fernandez, "Graphene oxide/silicon dioxide nanocomposites for electrochemical sensing applications," Nanomaterials, vol. 10, Art. no. 537, 2020, doi: 10.3390/nano10030537.

[31] X. Wei, J. Cruz, and W. Gorski, "Integration of enzymes and electrodes: Spectroscopic and electrochemical studies of chitosan–enzyme films," Anal. Chem., vol. 74, no. 19, pp. 5039–5046, 2002.

[32] M. George, S. S. Nair, K. Malini, P. Joy, and M. Anantharaman, "Finite size effects on the electrical properties of sol–gel synthesized $CoFe_2O_4$ powders: Deviation from Maxwell–Wagner theory and evidence of surface polarization effects," J. Phys. D: Appl. Phys., vol. 40, no. 6, Art. no. 1593, 2007.

[33] R. J. Sengwa and S. Choudhary, "Dielectric properties and structural dynamics of melt-

compounded hot-pressed poly (ethylene oxide)–organophilic montmorillonite clay nanocomposite films," Bull. Mater. Sci., vol. 35, no. 1, pp. 19–25, 2012.

[34] R. C. Agrawal and R. K. Gupta, "Superionic solids: Composite electrolyte phase—An overview," J. Mater. Sci., vol. 34, no. 6, pp. 1131–1162, 1999.

[35] H. D. Colorado and G. A. P. Alcázar, "Fe content and calcination temperature effects on CuO nanoparticles," Hyperfine Interact., vol. 241, no. 1, Art. no. 51, 2020, doi: 10.1007/s10751-020-01720-4.

[36] R. J. Sengwa and S. Choudhary, "Dielectric properties and structural dynamics of melt-compounded hot-pressed poly (ethylene oxide)–organophilic montmorillonite clay nanocomposite films," Bull. Mater. Sci., vol. 35, no. 1, pp. 19–25, 2012.

[37] Note: References 33 and 36 are duplicates of the same publication. In an IEEE reference list, only one should be retained. Additionally, references 23, 24, 25, 26, and 27 are incomplete in the original list, so the IEEE formatting above is based on the information you provided; if you have the full bibliographic details, I can produce fully accurate IEEE citations.